17th World Conference on Earthquake Engineering, 17WCEE
Sendai, Japan - September 13th to 18th 2020

A DAMAGE INDEX FOR THE POST-EVENT EVALUATION OF BUCKLING-RESTRAINED BRACES

J.A. Oviedo-Amezquita[(1)], N. Jaramillo-Santana[(2)], C.A. Blandon-Uribe[(3)], A.M. Bernal-Zuluaga[(4)]
[(1)] *Director, Seismic Protection Department, F'C Control & Design of Structures SAS, joviedo@efeprimace.co*
[(2)] *Coordinator, Seismic Protection Department, F'C Control & Design of Structures SAS, njaramillo@efeprimace.co*
[(3)] *Professor, EIA University, carlos.blandon@eia.edu.co*
[(4)] *Director, Structural Design Department, F'C Control & Design of Structures SAS, abernal@efeprimace.co*

Abstract

This paper focuses on the post-event evaluation of buckling-restrained braces (BRBs), in order to evaluate whether the BRB element should be replaced after a loading event. For this purpose, a damage index is proposed based on the experimental data obtained from a series of tests conducted on different BRB specimens. In total 19 full-scale BRB specimens were manufactured with local industry and workforce, and tested: 14 BRB specimens for a so-called low-cycle loading protocol, and five BRB specimens for a so-called high-cycle fatigue loading protocol. The specimens were designed having differential deformation and energy dissipation capacities. The low-cycle loading protocol slightly differs from that specified in the Colombian seismic code (NSR-10). For the high-cycle fatigue protocol, the axial strain at BRB core was increased from zero to 1.50%, and continued at 1.5% strain until core failure occurred. The proposed damage index has been calibrated based on the experimental results, and is capable of considering the effect of the maximum core strain attained as well as the cumulative deformation effect. A qualification scale has been assigned to the proposed damage index as a tool for evaluating whether the BRB element should be replaced or left on site. Furthermore, a series of nonlinear dynamic analyses were carried out on a sample building in order to validate the proposed damage index when subjected to ground motions. The results provided sufficient arguments to conclude that: (1) the proposed damage index varies from zero to slightly over one, in which a damage index larger or equal than unity represents the ultimate state of the BRB element, (2) a damage index lower than 0.30 indicates that the BRB element can be left on site with a reasonable safety margin against future events, (3) a damage index greater than 0.70 indicates that the BRB should be replaced, and (4) a damage index in the range of 0.30 and 0.70 indicates a BRB element that can be replaced or not, depending on a case-by-case analysis and on the building´s owner decision. Finally, the results suggest that the proposed damaged index can be useful in structural design practice.

Keywords: buckling-restrained brace; hysteretic damper; damage index; fatigue; experimental test

1. Introduction

As design methodologies and techniques advance, structural design philosophies point beyond the control of the collapse of building structures, and focus therefore on assessing the performance of buildings at different levels of seismic demand in order to meet heritage, interior furnishing and non-structural elements protection needs, building functionality, as well as to ensure the post-earthquake operation of essential buildings.

Among modern design philosophies, the Performance-Based Seismic Design methodology (PBSD), a design based on the behavior of the structure considering the concept of damage tolerance in structural, non-structural and building equipment component, has become very popular. This design philosophy allows the evaluation of the seismic reliability of buildings against earthquakes, and has been widely used for the design and retrofitting of building structures based on different guidelines and design codes [1-5]. In general, building structures designed under the PBSD concept have a higher level of reliability than those in which this concept has not been applied. One key aspect when evaluating the seismic performance of a building structure under the PBSD methodology has to do with the definition of the acceptance criteria for structural elements for a particular performance level; the ASCE 41-17 [5] document presents the acceptance criteria for several structural elements and materials. A complementary procedure for assessing the seismic performance of a structural element or a whole system is through the use of a damage index qualification. To date, many methodologies for damage index determination are available, particularly for reinforced-concrete and steel members [6-9].

The use of Buckling-Restrained Braces (BRBs) in building structures is still gaining popularity as an interesting alternative for the seismic design and retrofitting of building structures. In [10], the authors presented an evaluation of the reliability of two 24-story buildings. This study compared two steel buildings, one corresponding to the traditional structural system of ductile steel frames combined with moment-resistant frames (designed by conventional methods), and another with buckling-restrained braces. They reported a greater seismic reliability for the building incorporating BRB devices. Several studies are still being published reporting not only advances in the development of BRB elements, but also in the design methodologies (e.g., [11-20]. Recently, [21] presented the seismic performance assessment for a suite of buckling-restrained braced frames (BRBFs) in which they recommended that the acceptance criteria for BRBs listed in the ASCE 41 be re-examined. Therefore, the authors proposed an adjustment factor to account better for the cumulative deformation effect and the maximum deformation capacity of BRBs. In this work, however, no influence of BRB properties such as the plastic length was considered.

This paper is part of a larger investigation aimed at introducing two methodologies, one for defining the acceptance criteria for BRBs and another for determining a damage index (DI) when BRBs are subjected to seismic actions. Both methodologies have been established based on a set of experimental results [22-24] obtained from a series of tests carried out on a BRB prototype developed in Colombia. Thus, the present work introduces the methodology for the DI determination, targeted at the post-earthquake evaluation of BRB elements, and as a tool to determine whether the BRB should be replaced or not. The results of this study are expected to contribute to ongoing efforts on improving PBSD methodologies.

2. Testing Program

2.1 BRB specimens

In total 19 full-scale buckling-restrained braces (BRBs) were designed and manufactured with local industry and workforce. All BRBs were subjected to cyclic loading in tension and compression. Two types of loading protocol were considered: Protocol 1 corresponds to a more demanding loading protocol than the one required by the Colombian code, and the Protocol 2 corresponds to fatigue loading. The 19 specimens were divided and tested into three performance groups (PG). Table 1 shows the characteristics of each performance group and its research goals.

Table 1 - Performance groups for testing

Performance group (PG)	Prototypes	# specimen per prototype	Loading protocol	Research goal
I	PR1; PR2	3; 3	1	Global buckling
II	PR1; PR2 PR3; PR4	2; 2 2; 2	1	Plastic length, global buckling, unbonding gap
III	PR1; PR2	3; 2	2	Fatigue

Table 2 - Main structural characteristics of BRBs

PG /Prot.	Steel core						Buckling restrainer		
	w/t	A_{sc}	L_P ;	($\%L_B$)	P_y	δ_{By}	GB-SF	L_R	Gap
PGI / PR1	10.5	855	1,511;	(64)	248	-	2.10	1,797	0.8
PGI / PR2	10.5	855	1,511;	(64)	248	-	3.30	1,797	0.8
PGII / PR1	10.5	855	1,511;	(64)	248	2.53	3.28	1,797	0.5
PGII / PR2	10.5	855	705;	(30)	248	2.06	3.28	1,797	0.5
PGII / PR3	10.5	855	1,511;	(64)	248	2.53	4.72	1,797	0.5
PGII / PR4	10.5	855	1,511;	(64)	248	2.53	4.82	1,797	1.0
PGIII / PR1	10.5	855	1,261;	(54)	248	2.05	3.10	1,797	0.5
PGIII / PR2	10.5	855	705;	(30)	248	1.76	3.10	1,797	0.5

w/t: steel core width-to-thickness ratio
A_{sc}: steel core area, [mm^2]
L_P: plastic length: L_{P64} and L_{P30}, [mm]
$\%L_B$: L_P expressed as BRB length percentage
P_y: nominal yield strength, [kN]
δ_{By}: deformation between measuring points at core yield, [mm]
GB-SF: global buckling safety factor
L_R: buckling-restrained length, [mm]
Gap: Unbonding gap, [mm]

All prototypes have the same length (L_B=2,351 mm) and steel type (ASTM A-36), but they differ from each other in: (1) global buckling safety factor, (2) plastic length and (3) unbonding gap. Here, it is important to note that according to coupon test on the steel core, the yield stress for the PGI and PGII was 290 MPa, while 250 MPa for the PGIII. The tests carried out for PGs I and II aimed at understanding mainly the influence of the global buckling safety factor and the plastic length on the performance of the BRB prototype. The tests performed for the PGIII were carried out to understand the performance of prototypes under a fatigue-type loading. For this purpose, two prototypes of BRBs were designed and built; specifically, three specimens of PR1 and two of PR2, for a total of five BRB specimens. The main research goal was to study the effect of the loading protocol on the deformation and energy dissipation capacity of BRBs. Table 2 shows the structural characteristics of all 19 specimens, and the details on each group can be found elsewhere [22-24]. Fig. 1, on the right, illustrates the brace length (L_B), plastic length (L_P), buckling-restrained length (L_R) and the brace deformation between measuring points (δ_B). Fig. 1, on the left, illustrates the three different working zones into which the BRB is divided: Zone 1 corresponds to the elastic connection zone, Zone 2 corresponds to the elastic transition zone and the Zone 3 corresponds to the plastic zone (all axial inelastic deformation occurs within L_P). Fig. 2 shows the experimental set-up. It is worth mentioning that the brace deformation δ_B is considered to be adequate for practical use now that it can be readily measured on site through any displacement sensor or similar; brace deformation of Zone 1 is generally very small. δ_B includes the axial deformation of Zone 3 and both Zones 2.

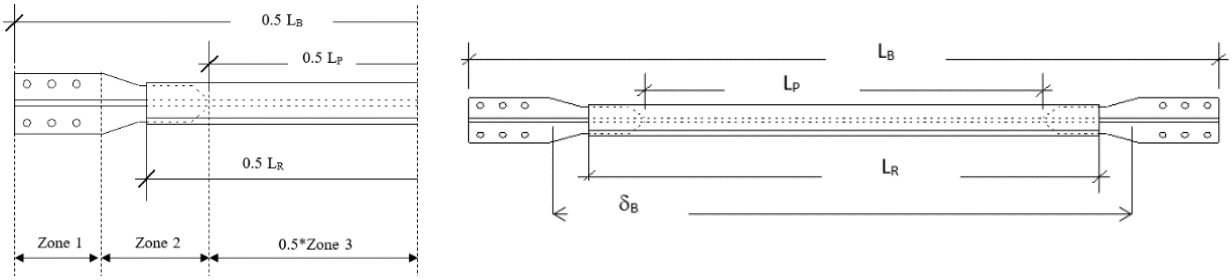

Fig. 1 – BRB definitions

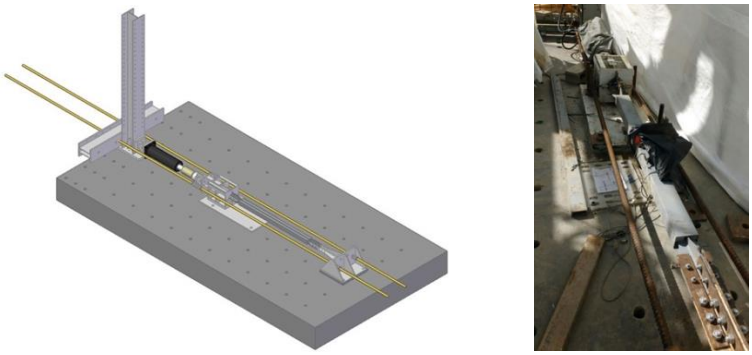

Fig. 2 – Experimental set-up

2.2 Loading protocol

As mentioned, two types of loading protocols were used in the testing program. Loading Protocol 1 (P1) was used for the PGs I and II, and the Loading Protocol 2 (P2) was used for the PGIII. All specimens were subjected to cyclic tensile and compressive loading in which the axial deformation in the plastic length of the brace was gradually increased from zero up to value of axial strain according to the protocol used.

In case of P1, the loading history used slightly differs from that stipulated in the Section F.3.11.3 of the Colombian Code NSR-10 [25]. It is worth mentioning that Section F.3.11.3 of NSR-10 is based on the protocol given by the document AISC 341-05 [26]. Thus, the P1 meets the conditions described in NSR-10 and the strain sequence is more demanding in terms of cumulative inelastic deformation. This loading protocol was chosen based on previous research programs carried out in Japan [13, 27] in order to obtain comparable data. Fig. 3a shows the loading protocol P1; it can be seen that axial strain of the steel core (ε_p) is increased from zero up to 3.0% strain.

In case of P2, all specimens of the PGIII were subjected to a cyclic tensile and compressive loading protocol in which the axial deformation in the plastic length of the brace was gradually increased from zero up to 1.5% axial strain, according to similar studies in other countries and current regulations [28, 29]. This protocol is divided into two parts: (1) 12 cycles with varying amplitude, similar to that of P1 until the axial strain reaches 1.5%, and (2) a sufficient number of cycles of constant amplitude of 1.5% axial strain, until failure is obtained. Fig. 3b shows the loading protocol P2, in which N_{c_f} stands for the cycle number at which failure occurred. Additional details of each loading protocol can be found elsewhere [22-24].

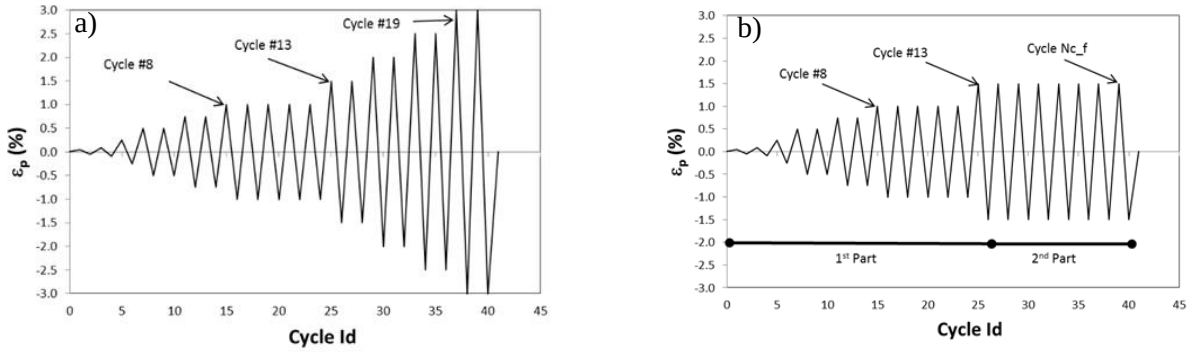

Fig. 3 – Loading protocols: a) P1, b) P2

2.3 Experimental results

Table 3 summarizes the experimental results obtained in the testing program for each performance group. Here, the results of the first three specimens of PGI tested have been intentionally left out the table due to some problems in the set-up at the time of the tests. Thus, in Table 3 η and ϖ stand for the cumulative plastic deformation and the cumulative strain energy, respectively. According to [12],η and ϖ are determined by Eq. (1) and Eq. (2), respectively (see Fig. 4).

$$\varpi = E_t / W_y = E_t / \left(P_y \delta_y\right) \tag{1}$$

$$\eta = \frac{\delta_1 + \delta_2 + \delta_3 + \cdots}{\delta_y} \tag{2}$$

In Table 3, ε_{max} and μ_{max} stand for the maximum axial core strain and maximum core ductility obtained in the test, respectively. β stands for the compression strength adjustment factor, and ω for the strain hardening adjustment factor. Here, it is important to mention that μ, η and ϖ are calculated over the length δ_B; thus, the ductility μ is given by Eq. (3).

$$\mu = \frac{\delta_B}{\delta_{By}} \tag{3}$$

Where, δ_B is the brace deformation between measuring points (see Fig. 1). Based on the results of all test conducted to the PGII, a limit for ε_p was set to 2.5% as a conservative deformation capacity for the BRB prototype, just before presenting local compression failure. Therefore, $\mu_{2.5}$ stands for the maximum ductility obtained at an axial strain equals to 2.5% (ε_p=0.025). Additional details on the response parameters obtained in all tests can be found elsewhere [22-24]. In Table 3, it is important to note that all specimens withstood a cumulative plastic deformation η greater than the value of 200 required by [25] and [30]. Moreover, it can be seen the significant increase in the cumulative plastic deformation and energy dissipation when the specimens are subjected to the fatigue protocol P2; specimens were able to increase in almost three times their response.

As for the failure mode of the specimens, experimental results showed that the specimens subjected to the P1 protocol failed mainly in a local-buckling failure mode in the steel core due to the capacity loss of the buckling restrainer. On the contrary, the specimens subjected to the P2 protocol failed in a tensile-fracture failure mode in the steel core due to fatigue. Here, it is important to mention that these two failure modes are accepted in case of BRB elements. Details on different failure modes can be found elsewhere [31, 32].

From Fig. 5, it is clear that the maximum ductility in the response history somewhat restrains the cumulative plastic deformation and energy dissipation. In other words, the larger the maximum axial strain (or ductility) in the response history, the lower the value of η and ϖ. This is to be expected since a large ductility demand imposes large forces on the buckling-restraining mechanism, leading it to failure. It is also

important to note that BRBs of PGII were able to withstand larger ductility demands than those of the PGI since a few changes in the prototype design were made to provide larger deformation capacity.

On the other hand, [33] established conservative limits for μ and η required on BRBs installed into a building structure: which are 15 and 200, respectively, in case of the design earthquake (DE) intensity, and 25 and 400, respectively, in case of the maximum considered earthquake (MCE). In the study, Life Safety (LS) performance level was considered for the DE earthquake and Collapse Prevention (CP) for the MCE earthquake. They also mentioned other experimental studies which have reported large values of cumulative plastic deformation (η = 1700); the results of η obtained in the PGIII are comparable with those large values.

In Fig. 5 it can also be observed that all PGIII specimens reached higher values of η than the limits proposed by [33] for the two levels of seismic intensity. In case of the specimens of the PGII, all reached values of η higher than the limit for the DE level, and a few specimens reached values higher than the limit for the MCE level. Here, the later corresponds to specimens having a larger plastic length (L_{P64}). This clearly indicates the great influence of L_P on the energy dissipation capacity.

Table 3 – Response parameters of tests

PG / Prototype	Spec.	η	ϖ	β	ω	ε_{max}(%)	η_{max}	$\eta_{2.5}$	N_{c-f}
PGI /PR2	2-1	259	259	1.09	1.26	1.5	9.40	N/A	N/A
PGI / PR2	2-2	357	304	1.14	1.29	2.0	12.52	N/A	N/A
PGI / PR2	2-3	324	301	1.09	1.26	2.0	12.39	N/A	N/A
PGII / PR1	1-1	594	518	1.27	1.20	3.0	17.64	15.12	N/A
PGII / PR1	1-2	431	527	1.19	1.37	2.5	15.51	15.51	N/A
PGII / PR2	2-1	287	291	1.02	1.19	3.0	10.93	9.18	N/A
PGII / PR2	2-2	345	366	1.07	1.34	3.0	11.29	9.55	N/A
PGII / PR3	3-1	359	367	1.01	1.35	2.5	15.22	15.22	N/A
PGII / PR3	3-2	486	554	1.24	1.40	3.0	18.16	15.18	N/A
PGII / PR4	4-1	544	643	1.12	1.50	3.0	18.21	15.17	N/A
PGII / PR4	4-2	597	746	1.25	1.41	3.0	18.72	15.60	N/A
PGIII / PR1	1-1	1,693	2,356	1.07	1.38	1.5	11.09	N/A	58
PGIII / PR1	1-2	1,868	2,356	1.07	1.26	1.5	10.93	N/A	64
PGIII / PR1	1-3	1,848	2,306	1.07	1.41	1.5	10.36	N/A	63
PGIII / PR2	2-1	1,354	1,508	1.04	1.15	1.5	7.65	N/A	70
PGIII / PR2	2-2	1,600	2,058	1.24	1.29	1.5	7.53	N/A	83

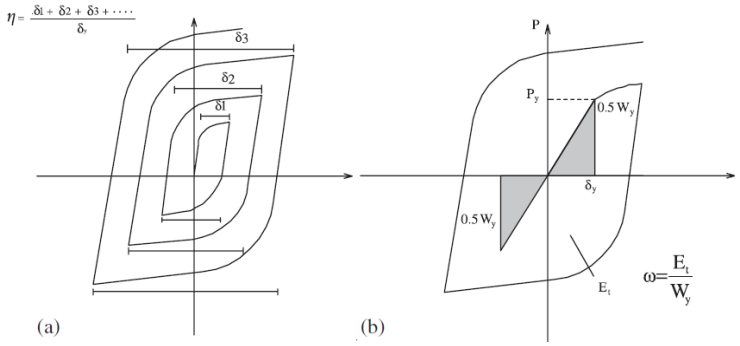

Fig. 4 – Definition of response parameters a) η, and b) ϖ, [12]

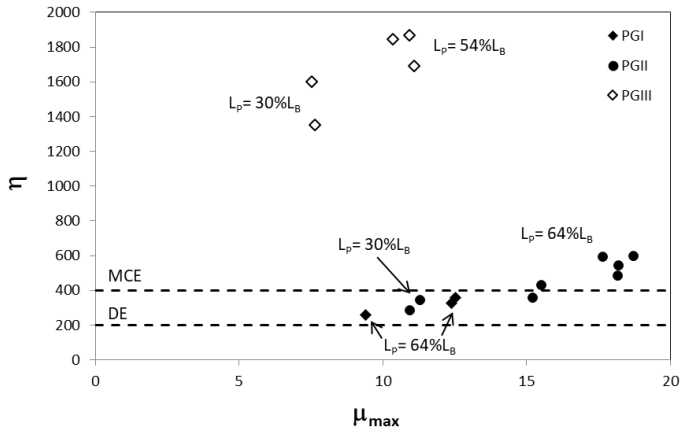

Fig. 5 – Response of parameters η and μ_{max}

3. Proposed Damage Index

Based on the test results, Eq. (4) is the proposed damage index (DI), which takes into account the two failure modes described in the previous section.

$$DI = {F_1}^{\alpha}\, {F_2}^{(1-\alpha)} \tag{4}$$

In Eq. (4), F_1 and F_2 are to represent the Type-A and Type-B failure modes, respectively. The α coefficient stands for a weighting factor, depending on the maximum axial deformation withstood between measuring points (δ_{Bmax}) and plastic length L_P. In Eq. (5), a and b coefficients are set to: a=0.5 (for equal participation of factors F_1 and F_2) and b= -15 (for better matching). It is important to note that experimental results showed that the contribution to the calculation of DI is an inversely-proportional type process between both failure modes. Thus, factors F_1 and F_2 can be determined by Eq. (6) and Eq. (7), respectively.

$$\alpha = a + b\frac{\delta_{Bmax}}{L_P} \tag{5}$$

$$F_1 = \frac{\delta_{Bmax}}{\delta_c} \tag{6}$$

$$F_2 = \frac{\eta_{max}}{\eta_c} \tag{7}$$

At the maximum demand, F_1 represents the effect of the maximum deformation, and F_2 represents the effect of cumulative plastic deformation. δ_c and η_c stand for the characteristic capacities observed under qualification tests, obtained from Eq. (8) a Eq. (9), respectively.

$$\delta_c = \delta_u - \sigma_\delta \tag{8}$$

$$\eta_c = \eta_u - \sigma_\eta \tag{9}$$

In Eq. (8) and Eq. (9), δ_u and η_u are the ultimate (maximum) deformation and ultimate cumulative plastic deformation measured in qualification tests, or at a particular "ultimate" state defined by the manufacturer, respectively. Here, δ_u was set to the brace deformation δ_B when ε_p reached 0.025, and η_u is the corresponding cumulative deformation obtained from Eq. (2). Here, it is worth recalling that specimens of the PGII were able to withstand axial core strains up to 0.030. Moreover, σ_δ and σ_η are the standard deviations for δ_u and η_u, respectively, among the qualification tests. It should be noted that a different set of (δ_c, η_c) is required for each plastic length L_P; η_c also depends on the failure type (or loading history type).

Table 4 shows the resulting characteristic capacities and the damage index calculation, while Fig. 6 depicts the evolution of damage index until failure. The resulting value of η_c shown in Table 4 varies between 80 to 90% of the ultimate average capacity (η_u) recorded in the tests, for both PGs II and III. On the other hand, the resulting value of δ_c varies between 95 to 100% of the ultimate average capacity (δ_u) recorded in the tests; this is because tests were performed under a displacement-controlled scheme.

Table 4 – Characteristic capacities and damage index

PG / Prototype	Spec.	η_c	δ_c (mm)	α	δ_{Bmax}/L_P	F_1	F_2	DI
PGII / PR1	1-1	398	38.24	0.118	0.025	1.01	1.29	1.25
PGII / PR1	1-2	398	38.24	0.110	0.026	1.02	1.08	1.08
PGII / PR2	2-1	261	18.73	0.100	0.027	1.05	1.01	1.01
PGII / PR2	2-2	261	18.73	0.085	0.028	1.04	1.05	1.05
PGII / PR3*	3-1	-	-	-	-	-	-	-
PGII / PR3	3-2	398	38.24	0.117	0.026	1.00	1.06	1.05
PGII / PR4	4-1	398	38.24	0.117	0.026	1.00	1.08	1.07
PGII / PR4	4-2	398	38.24	0.108	0.026	1.03	1.02	1.02
PGIII / PR1*	1-1	-	-	-	-	-	-	-
PGIII / PR1	1-2	1,833	32.50**	0.235	0.018	0.63	1.00	0.90
PGIII / PR1	1-3	1,833	32.50**	0.249	0.017	0.64	1.02	0.91
PGIII / PR2	2-1	1,321	18.73	0.205	0.020	0.74	1.03	0.96
PGIII / PR2	2-2	1,321	18.73	0.218	0.019	0.64	1.00	0.91

* Specimens were left out of calculation due to a minor premature failure observed in the tests (see [22, 23] for details). ** Extrapolated values

As seen in the last column of Table 4, DIs obtained from Eq. (4) can have values larger than unity; this is because characteristic values are taken conservatively smaller than the actual capacities measured in the tests. Another aspect to highlight has to do with the contribution of factors F_1 and F_2 to the DI; as expected, cumulative effect represented by the factor F_2 contributes more to the DI calculation in case of PGIII. As seen in Fig. 6, the evolution of DI varies with the loading protocol. In the PGII, the slope is larger and tends to remain constant until failure occurs, while in the PGIII, the slope tries to follow a bilinear behavior, slightly changing at a DI of about 0.2 to 0.3. The value of η equals to 200 corresponds to the minimum deformation capacity required for qualification testing [30]. From Fig. 6, the following DIs can then be assigned for $\eta = 200$: PGII: 0.5 for L_{P64} and 0.75 for L_{P30}; PGIII: 0.2 for L_{P54} and L_{P30}. It is again clear that the maximum deformation in the response history limits the cumulative plastic deformation; that is, the larger the maximum brace deformation (or ductility), the lower the cumulative plastic deformation capacity.

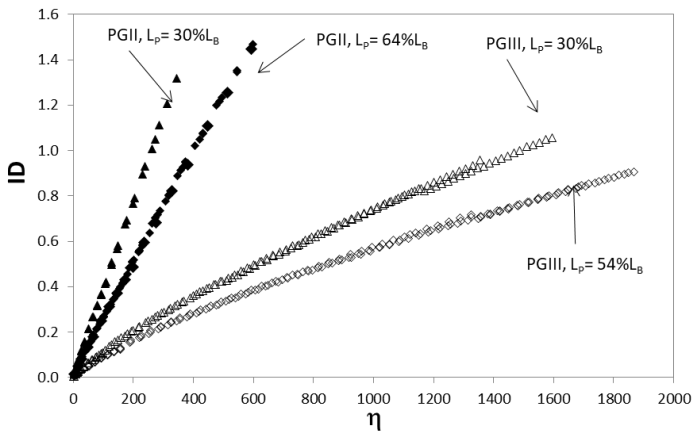

Fig. 6 – Evolution of damage index

As most damage indexes, the proposed DI requires a qualitative evaluation for design purposes. In case of BRBs, the evaluation should aim at defining whether a BRB specimen should be replaced or not after withstanding a particular loading history. Based on the test results, Table 5 shows a proposal for such an evaluation. Here, the limits DI=0.7 and DI=0.3 were also chosen to provide safety factors of about 1.5 and 3, respectively. Both safety factors are considered appropriate for accounting for capacity variations due to fabrication process.

Table 5 – Proposed damage index levels

Damage level	Damage index	Description
Severe	$DI \geq 0.7$	BRB should be replaced immediately.
Moderate	$0.3 \leq DI \leq 0.7$	BRB performance should be further investigated. Project owner's participation is required for deciding if the BRB is left on site or not.
Slight	$DI \leq 0.3$	BRB needs not be replaced. It could be replaced if physical damage is observed.

4. Results of Earthquake Response Analysis and Discussion

4.1 Studied sample building structure

A series of nonlinear dynamic analyses (NLDA) was carried out on a sample building in order to investigate the proposed damage index, when structures are subjected to earthquake motions. Fig. 7 shows the three-dimension six-story reinforced concrete (R/C) structure used as a sample building for dynamic analyses. The symmetric plan consists of 3 by 4 bays each of 7 m with a typical height of 3.5 m. The gravitational loads (dead and live) per unit area are assumed to be the same for all stories, with a typical superimposed dead load of 3.23 kN/m^2 and a typical live load of 4.0 kN/m^2 (for hospital use). Two pairs of BRBs in each direction were installed into the R/C main frame, as shown in Fig. 7; BRBs of each floor have the same structural properties. Thus, a total of 48 BRBs were installed into the R/C main frame, grouped into six different BRB types. The structural design was established based on the Colombian seismic code (NSR-10) for braced R/C moment-resisting frames, and BRBs were sized and designed according to the technical advised of the BRB manufacturer in Colombia. Table 6 summarizes the structural properties of the sample building. In Table 6, P_{ysc}, K_{Bwp} and K_{Bp} correspond to the yield strength (for a nominal yield stress of 250 MPa), workpoint-to-workpoint axial stiffness and post-yield axial stiffness of BRB. L_{Bwp} is the workpoint-to-workpoint length for braces. The total seismic weight of the three-dimension sample building is 29,742 kN, and the fundamental period is 0.68 s.

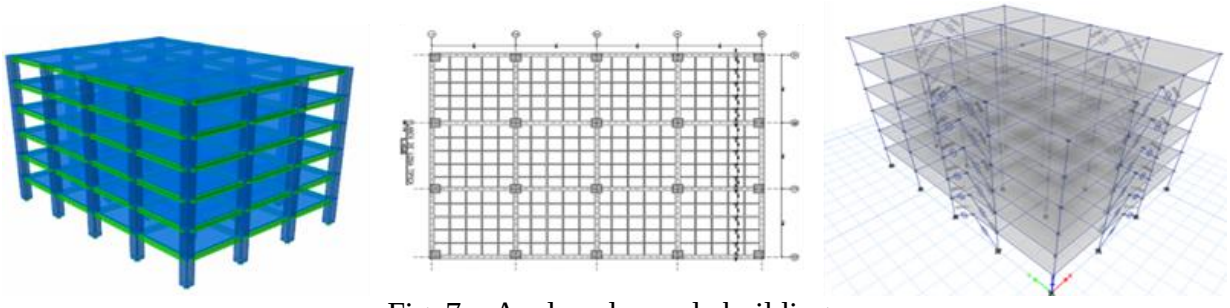

Fig. 7 – Analyzed sample buildings

4.2 Input ground motions and dynamic parameters

Three different acceleration records were selected for the nonlinear dynamic analysis (NLDA): Armenia (Colombia, 1999), Imperial Valley (USA, 1979) and Loma Prieta (USA, 1989). Two seismic levels were considered for the NLDAs, the DE and MCE earthquake levels. All records components were modified to match the DE design spectrum, according to requirements given by [25] and [34], and then were cut to retain

the 95% of the Arias intensity index [35]. Input motions for the MCE level were then multiplied by a factor of 1.5.

Table 7 summarizes the input motions used for the NLDAs, and Fig. 8 shows the response spectra of the spectrum-matched records. In Table 7, PGA-mod and Td correspond to the PGA of modified records and the time duration, respectively. The [36] computer program was used for all analyses, where BRBs were modeled trough nonlinear *Link* elements using the structural properties in Table 6 and a Wen type hysteresis model with a shape factor of 20. Here, only the degree of freedom for axial behavior of braces was activated, and links' both ends were considered as pin-end connections. Moreover, nonlinear hinges were assigned to each end of columns and beams; characteristics of the R/C plastic hinges were defined based on [5], through the feature of automatic hinges of the ETABS software. For all nonlinear analyses, the inherent viscous damping ratio is 0.02.

Table 6 – Structural properties of the analyzed sample building

Element	Section geometry (m)	Concrete strength (MPa)	P_{ysc} (kN)	K_{Bwp} ; K_{Bp} (kN/mm)
1st–6th story cols.	0.60 x 0.60	28	-	-
1st story braced frame cols.	0.70 x 0.70	28	-	-
1st–6th floor beams	0.40 x 0.55	21	-	-
1st story BRBs	L_{Bwp}= 4.95 L_B= 4.0 L_P= 2.4	-	1,125	300.5; 8.32
2nd story BRBs		-	1,575	420.6; 11.65
3rd story BRBs		-	1,260	336.5; 9.32
4th story BRBs		-	938	250.4; 6.94
5th story BRBs		-	540	144.2; 3.99
6th story BRBs		-	225	60.1; 1.66

Table 7 – Input ground motions for DE level

EQ. Source	Station	Input Motion	PGA (cm/s^2)	PGV (cm/s)	PGA-mod (cm/s^2)	Td (s)
Armenia	U.Quindio	A-1	580	251	358	17
		A-2	518	264	311	17
Loma Prieta	Corralito	LP-1	632	549	308	33
		LP-2	473	467	297	33
Imperial Valley	Cerro Prieto	IV-1	154	189	282	52
		IV-2	165	113	286	52

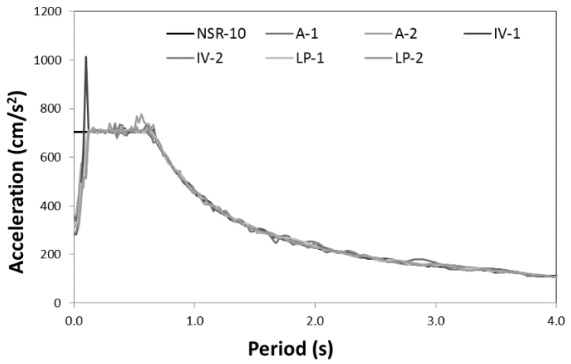

Fig. 8 – Response spectra of modified input motions for DE level

4.3 Damage index

Table 8 shows the earthquake demands and damage index obtained from Eq. (4) for the 1st-story BRBs. Values of Table 8 correspond to the maximum deformation demand among the three input motions.

Moreover, the Fig. 9a shows the force-deformation response of all braces of the first story under the MCE-IV input motion. Analysis results here are focused on the BRBs of the first story since they presented the higher earthquake demands. Values for δ_c and η_c were defined based on test result (see Section 3). Thus, δ_c was set to $0.90\delta_u$, where δ_u is the brace deformation (δ_B, see Fig. 1) when ε_P reaches 2.5%. As for η_c, it was set through linear interpolation from the available test results of Section 3. Thus, one value of η_c was defined for each protocol type: $\eta_c = 398$ for a P1-like protocol, and $\eta_c = 1{,}321$ for a P2-like protocol.

Fig. 9b shows the time history of δ_B normalized by δ_{By} for one 1st-story BRB under the IV input motion. It can be concluded from Fig. 9b that demands on BRBs correspond better to a P1-like loading protocol, rather than to a fatigue loading type. Therefore, $\eta_c = 398$ was then used for the DI calculation shown in Table 8. Moreover, the force-deformation response obtained in the PGII tests (details can be found in [23]) is also depicted in Fig. 9a for comparison. As seen in Fig. 9a, the force-deformation demand on BRBs are quite below the obtained BRB capacity; so, low values for DI shown in Table 8 agree reasonably well. Based on the calculated DI values and the criteria show in Table 5, the damage level for all eight BRBs is slight, and they can be left on site for future events.

Table 8 – Earthquake demands and DI for 1st-story BRBs

BRB ID	δ_{Bmax} (mm)	δ_{By} (mm)	δ_c (mm)	ε_{Pmax} (%)	η_{max}	α	F_1	F_2	DI
1 – X	8.22	3.74	54.6	0.34	14.62	0.4486	0.151	0.037	0.07
2 – X	8.88	3.74	54.6	0.37	13.80	0.4445	0.163	0.035	0.07
3 – X	8.57	3.74	54.6	0.36	17.79	0.4464	0.157	0.045	0.09
4 – X	9.02	3.74	54.6	0.38	15.53	0.4437	0.165	0.039	0.07
1 – Y	7.36	3.74	54.6	0.31	9.08	0.4540	0.135	0.023	0.05
2 – Y	7.36	3.74	54.6	0.31	9.32	0.4540	0.135	0.023	0.05
3 – Y	7.40	3.74	54.6	0.31	9.76	0.4537	0.136	0.024	0.05
4 – Y	7.40	3.74	54.6	0.31	8.00	0.4534	0.137	0.020	0.05

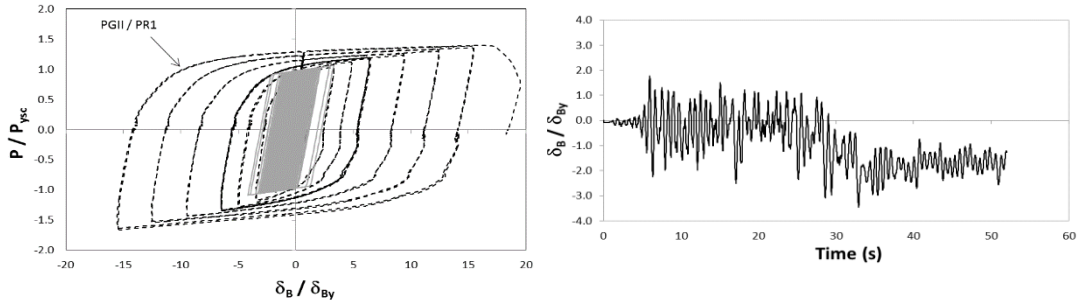

Fig. 9 – Response of 1st-story BRBs under the MCE-IV input motion: a) normalized force-deformation, and b) deformation time-history

5. Conclusions

A methodology for determining the damage index (DI) for BRBs, when subjected to seismic actions, have been introduced and validated through the nonlinear dynamic analysis of a sample building. The proposed damage index was established based on a set of experimental results obtained from a series of tests carried out on a BRB prototype developed in Colombia. From the results of this study, the proposed methodology for the damage index evaluation has proven to be a potential tool for the post-earthquake evaluation of the performance of a BRB element, and for determining whether the BRB should be replaced or left on site for future events. Further study for different types of BRB elements, other loading protocols and more building

archetypes is needed to gain more insight into this subject, and to validate the applicability of the proposed damage index. Finally, the results of this study are expected to contribute to ongoing efforts on improving PBSD methodologies.

6. References

[1]. Applied Technology Council (ATC). (1996): The Seismic Evaluation and Retrofit of Concrete Buildings. *ATC 40 Report*. Redwood City, California.
[2]. Federal Emergency Management Agency-FEMA (1997): NEHRP Guidelines for the Seismic Rehabilitation of Buildings (FEMA 273). *FEMA*, Washington, DC, USA.
[3]. Federal Emergency Management Agency-FEMA (2000): Prestandard and Commentary for the Seismic Rehabilitation of Buildings (FEMA 356). *FEMA*, Washington, DC, USA.
[4]. Federal Emergency Management Agency-FEMA (2003): NEHRP Recommended Provisions for Seismic Regulations for New Buildings and Other Structures (FEMA 450). *FEMA 2003 Edition*, Washington, DC, USA.
[5]. American society of Civil engineers. (2017): Seismic Evaluation and Retrofit of Existing Buildings. *ASCE/SEI 41-17*. Reston, Virginia, USA.
[6]. Park YJ, Ang A. (1985). Mechanistic seismic damage model for reinforced concrete. *Journal of Structural Engineering.* **111** (4), 740-775.
[7]. Mehanny SF, Deierlein GG. (2000). Modeling of assessment of seismic performance of composite frames with reinforced concrete columns and steel beams. *Report No. 135*, the John A. Blume Earthquake Engineering Center, Stanford University.
[8]. Cao,VV; Ronagh, HR; Ashraf,M; Baji, H, (2014): A new damage index for reinforced concrete structures. Earthquakes and Structures. **6** (6).
[9]. Bojórquez Mora, Edén, Terán Gilmore, Amador, Bojórquez Mora, Juan, & Ruiz Gómez, Sonia E. (2009). Consideración explícita del daño acumulado en el diseño sísmico de estructuras a través de factores de reducción de resistencia por ductilidad. Ingeniería sísmica, (80), 31-62.
[10]. Montiel-Ortega MA, Terán-Gilmore A (2008): Evaluación y comparación de la confiabilidad de edificios de 24 niveles estructurados con contravientos tradicionales y con contravientos restringidos contra pandeo. *XVI Congreso Nacional de Ingeniería Estructural (CD)*. Veracruz, Veracruz, México.
[11]. Chang RWK, Albermani F (2008): Experimental study of steel slit damper for passive energy dissipation. Engineering Structures, 30 (4), 1058-1066.
[12]. Iwata M, Murai M (2006): Buckling-restrained brace using steel mortar planks; performance evaluation as a hysteretic damper. Earthquake Engineering Structu*ral Dynamics*, **35** (14), 1807- 1826.
[13]. Wada A, Nakashima M (2004): From infancy to maturity of buckling restrained braces research. *Proceedings of the 13th World Conference on Earthquake Engineering*, Paper No. 1732, Vancouver, Canada.
[14]. Whittaker AS, Bertero VV, Alonso J, Thompson C (1989): Earthquake simulator testing of steel plate added damping and stiffness elements, *Report No. UCB/EERC-89/02.* Earthquake Engineering Research Center, University of California, Berkeley, California.
[15]. Oviedo JA, Midorikawa M, Asari T. (2008): Optimum strength ratio of buckling-restrained braces as hysteretic dissipation devices installed in R/C frames. The 14th World Conference on Earthquake Engineering, Vancouver, Canada.
[16]. Oviedo-A JA, Midorikawa M, Asari T (2010): Earthquake response of ten-story story drift-controlled reinforced concrete frames with hysteretic dampers. *Engineering Structures*, **32** (6), 1735-1746.
[17]. Oviedo JA. (2012): Influence of the story stiffness of reinforced concrete frame with proportional hysteretic dampers on the seismic response. Revista EIA. 17, 121-137.
[18]. Oviedo J, Buitrago J, Patiño J, Hoyos D (2015): Evaluación experimental del desempeño de un disipador de energía por deformación tipo riostra. *VII Congreso Nacional de Ingeniería Sísmica*, Bogotá, Colombia.
[19]. Oviedo J, Ortiz N, Blandón C (2017): Evaluación experimental del comportamiento de riostras restringidas contra pandeo fabricadas en Colombia. *VIII Congreso Nacional de Ingeniería Sísmica*, Barranquilla, Colombia.
[20]. Oviedo-Amézquita JA, Jaramillo-Santana N, Blandón-Uribe CA. (2019): Evaluación experimental bajo condiciones de fatiga de riostras restringidas contra pandeo fabricadas en Colombia/ Fatigue experimental evaluation of buckling-restrained braces fabricated in Colombia. *IX Congreso Nacional de Ingeniería Sísmica*. Cali, Colombia.
[21]. Speicher MS, Harris JL. (2018): Collapse prevention seismic performance assessment of new buckling restrained braced frames using ASCE 41. Engineering Structures. **164**, 274-289.
[22]. Oviedo-A JA (2015): Desempeño de un elemento estructural de disipación de energía por deformación para F'C Control y Diseño de Estructuras SAS - FASE I. *Reporte por F'C SAS*, Medellín, Antioquia, Colombia.
[23]. Oviedo-A JA (2017): Desempeño de un elemento estructural de disipación de energía por deformación para F'C Control y Diseño de Estructuras SAS - FASE II. *Reporte por F'C SAS*, Medellín, Antioquia, Colombia.
[24]. Oviedo-A JA (2018): Desempeño de un elemento estructural de disipación de energía por deformación para F'C Control y Diseño de Estructuras SAS - FASE III. *Reporte por F'C SAS*, Medellín, Antioquia, Colombia.
[25]. Asociación Colombiana de Ingeniería Sísmica -AIS- (2017): *Reglamento Colombiano de Construcciones Sismo Resistente NSR-10.* Bogotá D.C., Colombia.
[26]. American institute of steel construction, Inc. (2005): Seismic Provisions for structural steel buildings. *ANSI/AISC 341-05*. Chicago, Illions, USA.
[27]. Iwata M, Murai M (2006): Buckling-restrained brace using steel mortar planks; performance evaluation as a hysteretic damper. *Earthquake Engineering Structural Dynamics*, **35** (14), 1807- 1826.
[28]. Tsai K, Lai J, Hwang Y, Lin S, Weng C. (2004): Research and application of double-core buckling restrained braced in Taiwan. Proceedings of the 13th world conference on earthquake, Vancouver, Canada.
[29]. Usami T, Wang C, Funayama J (2011): Low-cycle fatigue tests of a type of buckling restrained. *The Twelfth East Asia-Pacific Conference on Structural Engineering and Construction*. Hong Kong, China.
[30]. American Institute of Steel Construction (2010): Seismic provisions for structural steel buildings. *ANSI/AISC 341-10*, Chicago, Illinois, USA.
[31]. Takeuchi T, Wada A. (2017): Buckling-restrained braces and applications. *The Japan society of seismic isolation, JSSI*, Tokyo, Japan.
[32]. Wei C, Tsai K (2008): Local buckling of buckling-restrained braces. *Proceedings of the 14th World Conference on Earthquake Engineering*. Bejing, China.
[33]. Fahnestock LA, Sause R, Ricles JM. (2006). Analytical and Large-Scale Experimental Studies of Earthquake-Resistant Buckling-Restrained Braced Frame Systems" (2006). *ATLSS Reports. ATLSS report number 06-01*:. http://preserve.lehigh.edu/engr-civil-environmental-atlss-reports/71.
[34]. American society of Civil engineers. (2017): Minimum Design Loads and Associated Criteria for Buildings and Other Structures (ASCE/SEI 7-16)
[35]. Arias A. (1970): A Measure of Earthquake Intensity. In: *Seismic Design for Nuclear Power Plants* by Hansen RJ (ed.), The MIT Press, Cambridge, MA, 438–483.
[36]. Computers & Structures, Inc. (2017): Structural and Earthquake Engineering Software, ETABS v17.0.1. https://www.csiespana.com/software/5/etabs

